Journal of Catalysis 262 (2009) 266–279

Contents lists available at ScienceDirect

Journal of Catalysis

www.elsevier.com/locate/jcat

The interfacial chemistry of the impregnation step involved in the preparation of tungsten(VI) supported titania catalysts

George D. Panagiotou [a], Theano Petsi [a], Kyriakos Bourikas [a,b,*], Christos Kordulis [a,c], Alexis Lycourghiotis [a]

[a] Department of Chemistry, University of Patras, GR-265 00 Patras, Greece
[b] School of Science and Technology, Hellenic Open University, Sahtouri 16, GR-26222, Patras, Greece
[c] Institute of Chemical Engineering and High-Temperature Chemical Processes (FORTH/ICE-HT), P.O. Box 1414, GR-265 00 Patras, Greece

ARTICLE INFO

Article history:
Received 7 October 2008
Revised 26 December 2008
Accepted 6 January 2009
Available online 23 January 2009

Keywords:
Titanium oxide
Preparation of tungsten supported titania catalysts
Interfacial chemistry
(Hydr)oxo-groups
Surface complexes
Adsorption
Interface
Surface charge
Zeta potential
Laser-Raman spectroscopy

ABSTRACT

An integrated work concerning the interfacial chemistry of the impregnation step involved in the preparation of tungsten(VI) supported titania catalysts is presented. Specifically, we investigated the mode of interfacial deposition of the W(VI) oxo-species at the "titania/impregnation solution" interface, the W(VI) interfacial speciation and the structure of the deposited species. Several methodologies based on potentiometric titrations, microelectrophoresis and macroscopic adsorption measurements have been used in conjunction with laser Raman spectroscopy and a modeling of the interfacial deposition process. The modeling was based on a recently established ionization model for the titania surface and a modern picture for the "titania/electrolytic solution" interface in the absence of the W(VI) oxo-species. It was found that the monomers, WO_4^{2-}, are exclusively deposited at the interface at relatively low W(VI) concentrations of the impregnation solution ($\leqslant 10^{-3}$ M) and over the whole pH range studied (9–4). Three different monomers are formed: an inner sphere mono-substituted complex with the terminal surface oxygen atoms of titania (predominant species), a surface species where the WO_4^{2-} ions are retained above a bridging surface hydroxyl through a hydrogen bond and an inner sphere di-substituted complex with two terminal surface oxygen atoms of titania. Their relative surface concentration depends strongly on the pH of the impregnation solution. At relatively high W(VI) concentrations of the impregnation solution ($>10^{-3}$ M) the polymers $W_7O_{24}^{6-}$, $HW_7O_{24}^{5-}$ and $H_2W_{12}O_{42}^{10-}$ are deposited, in addition, in the pH range 7–4. These species are adsorbed through electrostatic forces on adsorption sites that involve 5–7 bridging and 5–7 terminal neighboring (hydr)oxo groups. It was generally found a preferential deposition of the monomers, WO_4^{2-}, with respect to the polymer ones. The mode of interfacial deposition, the interfacial speciation and the structure of the deposited W(VI) oxo-species, would be very useful for a tailor made preparation of the tungsten supported titania catalysts.

1. Introduction

Tungsten(VI) supported titania catalysts are increasingly promising functional materials for many reactions of environmental interest. The SCR of NO_x [1–3], the removal of various pollutants such as chloro-organic compounds [4], chloro/fluoro-carbons (CFC-12) [5], dibenzodioxins and dibenzofurans [6] and the hydrodesulfurization reactions [7] should be mentioned. The WO_3/TiO_2 catalysts are, moreover, suitable for certain photocatalytic reactions such as the photooxidation of methane [8] and the photodegradation of 4-nitrophenol [9], of methyl orange [10] and of 1,4-dichlorobenzene [11]. Finally, tungsten(VI) supported titania catalysts are promising functional materials for several reactions of industrial interest such as the acid catalyzed dehydration of 2-propanol and dealkylation of cymene [12] as well as the metathesis and isomerization of alkenes [13,14].

The catalytic behavior of a supported catalyst based on a given support depends largely on the physicochemical characteristics of the supported active species or supported nanoparticles. Suitable physicochemical characteristics and thus catalytic behavior for a given reaction may be obtained by controlling the preparation procedure, *mainly the initial impregnation step* [15–24]. In order to obtain such a control and put to a scientific base the art of the catalyst preparation it is necessary to understand *at a molecular level* the fundamental processes taking place in the impregnation step. This mainly concerns the "equilibrium deposition filtration (EDF)" [15] and the "homogeneous deposition-precipitation (HDP)" [25,26] techniques which favor deposition, upon the equilibration of the suspension, at *the interface* developed between the surface

* Corresponding author at: Department of Chemistry, University of Patras, GR-265 00 Patras, Greece. Fax: +302610994796.
E-mail address: kmpo@chemistry.upatras.gr (K. Bourikas).

0021-9517/$ – see front matter
doi:10.1016/j.jcat.2009.01.003

of the support grains and the solution (*interfacial deposition*) and to a lesser extent the conventional *incipient wetness impregnation (IWI)* or *wet impregnation (WI)* techniques [15,16]. The close relation between the species formed upon impregnation and the characteristics of the final active phase has been explained in detail in an extensive article recently reported by our group [15]. In spite of its importance, the title impregnation step has not been yet studied. The work reported so far concerned preparation by IWI or WI and characterizations mainly *after calcinations* [27–31]. On the other hand works dealing with the deposition of the W(VI) oxo-species on other supports are not abundant in the literature [32–37]. Most of them concern the deposition of the W(VI) oxo-species on the γ-alumina surface.

The understanding in depth of the interfacial chemistry of the impregnation step involved in the preparation of tungsten(VI) supported titania catalysts *requires prior achievement of a mapping of the titania (hydr)oxo-groups, considered as the receptor sites for the deposition of the W(VI) oxo-species, and of the "titania/electrolyte solution" interface* as well. This has been recently reported by our group [38]. According to the surface ionization model established (Fig. 29 of Ref. [38]), two kinds of oxo-groups with different charges and protonation constants are developed on the titania surface: the terminal oxo-groups ($TiO^{-0.35}$) and the bridging ones ($Ti_2O^{-0.57}$). Both may undergo one protonation step transforming into ($TiOH^{+0.65}$) and ($Ti_2OH^{+0.43}$), respectively. The interface is divided by three charged planes into three sub-regions (Fig. 33 of Ref. [38]). The surface plane is located at the oxygen atoms of the (hydr) oxo-groups. Plane 1 is located at the oxygen atoms of the first layer of ordered water molecules surrounding the titania surface. Plane 2 is located at the center of the second layer of the ordered water molecules. The first two regions constitute the so called "compact layer" of the interface. The distance between the surface plane and the plane 1 as well as the distance between the plane 1 and the plane 2 is 1.7 Å. The third sub-region, up to bulk solution, is called diffuse *layer* where the indifferent-counter ions are accumulated. A portion of these ions is also located inside the compact layer forming ion-pairs with the surface (hydr)oxo groups of opposite charge. The *shear plane* divides the interface into two parts: the stagnant one (comprised from the compact layer and the *stagnant-diffuse layer*), which "accompanies" the titania aggregates when they are moved under the influence of an electric field by applying an electrokinetic technique, and the external part which is separated from the moving aggregates (*mobile-diffuse layer*). The aforementioned picture for the titania surface and the "titania/electrolyte solution" interface was developed by taking into account a certain contribution of the (1 0 1), (1 0 0), (0 0 1) anatase and (1 1 0) rutile perfect crystal faces to the whole surface area of the titania nanocrystals. Moreover, it was based on charges of the surface oxygen atoms determined using density functional theory ab initio calculations [38].

In this paper we present an integrated work concerning the interfacial chemistry of the impregnation step involved in the preparation of tungsten supported titania catalysts. This is based on the aforementioned study [38]. Specifically, we investigate the mode of interfacial deposition of the W(VI) oxo-species at the "titania/impregnation solution" interface (e.g. electrostatic adsorption, formation of surface hydrogen bonds, formation of surface inner sphere complexes etc.), the interfacial speciation and the surface structure of the deposited W(VI) oxo-species. Several methodologies based on potentiometric titrations, microelectrophoresis and macroscopic adsorption measurements have been used in conjunction with laser Raman spectroscopy. The latter has been proved a useful tool in the determination of both the interactions between support surfaces and transition metal ionic species (TMIS) and the surface structure of these species [39]. The aforementioned methodologies were followed by a quantitative modeling of the interfacial deposition process.

2. Experimental

2.1. Substances

$NaNO_3$ dissolved in triply distilled CO_2-free water and $Na_2WO_4 \cdot 2H_2O$ were used for the preparation respectively of the indifferent electrolyte and impregnating solutions necessary for the deposition, microelecrophoresis, proton–ion, pH-equilibrium and potentiometric titration experiments. $(NH_4)_{10}W_{12}O_{41} \cdot 5H_2O$ was used in the laser-Raman experiments.

2.2. Support

Industrial titania (Degussa P25) containing (80%, w/w) anatase and 20% (w/w) rutile was used for preparing the suspensions in all cases. Its surface composition is ≈90% anatase and only ≈10% rutile [40,41]. XRD spectra indicated that this material is constituted from primary nanocrystals of about 20 nm. A similar size for these nanocrystals (30–40 nm) was determined by SEM images. The application of the laser scattering technique showed that these are assembled into aggregates of various sizes, mainly in the range 0.5–10 μm (81%) with a distribution centered at about 8 μm.

The textural analysis, carried out using a Micromeritics Gemini III 2375, showed a BET specific surface area of 50 m^2/g, the major portion of which, 32 m^2/g, is due to the pores in the range of 1.7–300 nm with a total specific pore volume equal to 0.14 cm^3/g. The BET and BJH average pore diameters were found to be equal to 15.4 and 17.2 nm, respectively. The average pore diameters indicate that most of the pores are formed between the primary nanocrystals.

2.3. Equilibrium deposition experiments

2.3.1. The set-up used in the deposition and potentiometric titrations experiments

A thermostated double walled Pyrex vessel equipped with a magnetic stirrer and a perspex lid with holes for electrodes and nitrogen gas was used. The control (change) of the pH during the deposition (titration) experiments was carried out by an automatic microburette (Radiometer Copenhagen ABU901 Autoburette) equipped with a combination pH electrode. The experiments were performed at $25 \pm 0.1\,^{\circ}C$ and ionic strength 0.1 M adjusted by sodium nitrate. Nitrogen gas was passed into the vessel during the experiments to prevent the dilution of the atmospheric CO_2, which would bring about a change in the pH.

2.3.2. Adsorption edges

Adsorption edges were done at two different initial W(VI) concentrations (10^{-2} and 2×10^{-2} M). Details concerning the experimental procedure can be found elsewhere [42].

2.3.3. Adsorption isotherms

Adsorption isotherms were done at six pH values (4, 5, 6, 7, 8, 9). At each isotherm the initial W(VI) concentrations varies in the range 3.5×10^{-4}–3.5×10^{-2} M. Details about the experimental procedure can be found elsewhere [32].

In all adsorption experiments the equilibrium W(VI) concentration in the impregnation solutions was determined spectrophotometrically at 403 nm [43].

2.4. Proton–ion titrations at constant pH

Proton–ion titrations were performed at six pH values (4, 5, 6, 7, 8, 9) under conditions where an almost complete deposition of the W(VI) is obtained. In fact, under certain experimental

conditions (high solid to liquid ratio, low W(VI) solution concentration) the solution W(VI) concentration after deposition is negligible compared to that deposited on the titania surface. Details for the experimental procedure can be found elsewhere [42].

2.5. Equilibrium pH experiments

In each equilibrium deposition experiment, the change of pH upon deposition was measured. The experiments were performed for various initial W(VI) concentrations at three different pHs (pH 9 (initial W(VI) concentrations: 10^{-4}, 10^{-3}, 4×10^{-3}, 7×10^{-3}, 10^{-2} M), pH 7 (initial W(VI) concentrations: 10^{-4}, 5×10^{-4}, 10^{-3}, 2×10^{-3}, 4×10^{-3} M) and pH 5 (initial W(VI) concentrations: 10^{-4}, 4×10^{-4}, 7×10^{-4}, 10^{-3}, 2×10^{-3}, 3×10^{-3} M)).

2.6. Electrochemical techniques

2.6.1. Potentiometric titrations at different ionic strengths

The conventional potentiometric titration technique was used for determining the point of zero charge of the suspensions, both in the presence and absence of the W(VI) oxo-species to be deposited. Following this methodology potentiometric titrations were performed, under N_2 atmosphere, at three different values of the ionic strength (0.1, 0.01 and 0.001 M) and constant temperature (25.0 ± 0.1 °C). Details about the experimental procedure and the derivation of "surface charge density vs pH" curves can be found elsewhere [44,45]. It must be noted that the potentiometric titrations in the presence of the W(VI) oxo-species were performed at a W(VI) concentration equal to 5×10^{-5} M, where the whole amount of the W(VI) oxo-species is practically deposited at the interface.

2.6.2. Microelectrophoresis experiments

The ζ potential of the suspensions was determined both in the absence and presence of the W(VI) oxo-species at five different initial W(VI) concentrations using a Zetasizer 5000 (Malvern Instruments Ltd.) microelectrophoresis apparatus. At each initial W(VI) concentration the ζ potential was determined in the pH range 2.5–9.5. Details for the experimental procedure can be found elsewhere [44].

2.7. Laser-Raman spectroscopy (LRS)

The laser-Raman spectra of the support, the solids $Na_2WO_4\cdot2H_2O$ and $(NH_4)_{10}W_{12}O_{41}\cdot5H_2O$, the $Na_2WO_4\cdot2H_2O$ and $(NH_4)_{10}W_{12}O_{41}\cdot5H_2O$ aqueous solutions at various pHs as well as of the various $H_kW_XO_Y^{Z-}/TiO_2$ wet and dried solid samples were recorded in the range 0–1400 cm^{-1} at room temperature, using a micro-Raman system (model T-6400, Jobin Yvon). The $H_kW_XO_Y^{Z-}/TiO_2$ wet solid samples were selected after filtering the samples taken at various pH values (9, 8, 7, 6, 5, 4) during the adsorption edge experiment, at initial W(VI) concentration equal to 2.8×10^{-2} M. This initial concentration corresponded to the plateau of the adsorption isotherms at which the deposition was maximized for a given pH. Besides the LR spectra of the aforementioned wet samples, the LR spectra of the corresponding dried samples have been also taken. The samples were dried at 115 °C for 1 h. Moreover, the LR spectra were recorded for $H_kW_XO_Y^{Z-}/TiO_2$ wet solid samples taken at the end of the *proton–ion titrations* at constant pH. This was done for two pH values (4, 5). Each sample was filtered and the LR spectra were recorded for the liquid and solid (*wet*) part of each sample.

2.8. Simulations

The simulations (quantitative modeling) relevant to the proton–ion, and deposition isotherms results were carried out using Visual MINTEQ, a computer code for the calculation of chemical equilibria in aqueous media [46]. The modeling takes into account the mass and the charge balance equations as well as the equilibrium equations for each species being at the various planes (or layers) of the interface and in the solution as well (see Appendix A2 in Supplementary material).

3. Results

3.1. Speciation of the W(VI) in the solution

The W(VI) oxo-species more probably present in the solution are: WO_4^{2-}, HWO_4^-, $WO_3(H_2O)_3$, $H_2W_6O_{22}^{6-}$, $W_7O_{24}^{6-}$, $HW_7O_{24}^{5-}$ and $H_2W_{12}O_{42}^{10-}$. These species and their formation constants have been incorporated in several computer codes [e.g., 46]. The application of these codes allows the determination of the *solution speciation*, namely the concentration of each species at any pH and concentration of the transition metal. The determination of the W(VI) speciation under conditions *similar to those of the deposition experiments* is actually needed. This was achieved using the computer code Visual MINTEQ [46] (see Appendix A1 in Supplementary material).

It was found that for W(VI) concentrations $\leqslant3\times10^{-4}$ M and pH > 6.5 practically, the only W(VI) species present in the solution are the tetrahedral monomers (WO_4^{2-}). The decrease of pH brings about polymerization and transformation of the WO_4^{2-} ions into the doubly protonated hexacoordinated $WO_3(H_2O)_3$ species. The later predominate at pHs < 3. Concerning the polymer species the $HW_7O_{24}^{5-}$ and $W_7O_{24}^{6-}$ ions are the most abundant, whereas the concentration of the $H_2W_{12}O_{42}^{10-}$ ions becomes considerable for W(VI) concentration equal to 3×10^{-4} M. For W(VI) concentrations in the range 3×10^{-3}–3×10^{-2} M, the species present in the solution are the tetrahedral monomers (WO_4^{2-}) when pH > 7. Decrease in pH brings about polymerization. It was found that $HW_7O_{24}^{5-}$, $W_7O_{24}^{6-}$ and $H_2W_{12}O_{42}^{10-}$ ions are the most abundant among the polymer species. More details concerning the solution speciation achieved are illustrated in Figs. A1-1–A1-4 of Appendix A1 in Supplementary material.

3.2. Deposition experiments

The adsorption isotherms obtained for various pH values and over a broad initial W(VI) concentration range are illustrated in Fig. 1.

It may be seen that the surface W(VI) concentration, Γ_W, increases with the initial W(VI) concentration in the solution. Moreover, it increases as pH decreases. The first observation is expected whereas the second will be discussed in Section 4.

The change of pH upon the deposition of the W(VI) oxo-species at the "titania/impregnating solution" interface is depicted in Fig. 2. A considerable increase of pH may be observed.

3.3. Electrochemical techniques

The variation of the surface charge density of the titania aggregates with pH in the presence of the W(VI) oxo-species in the impregnating suspension is illustrated in Fig. 3. Taking into account that the pzc of titania is equal to 6.5 one may observe a significant shift of the pzc to a higher value (8.4).

The ζ potential curves, both in the absence and presence of the W(VI) oxo-species, are presented in Fig. 4.

These curves illustrate the variation, with pH, of the potential at the shear plane of the interfacial region. The isoelectric point (iep) is the pH value where this parameter takes a zero value. It may be seen that the presence of the W(VI) oxo-species in the suspension decreases the ζ potential and shifts the iep to lower values.

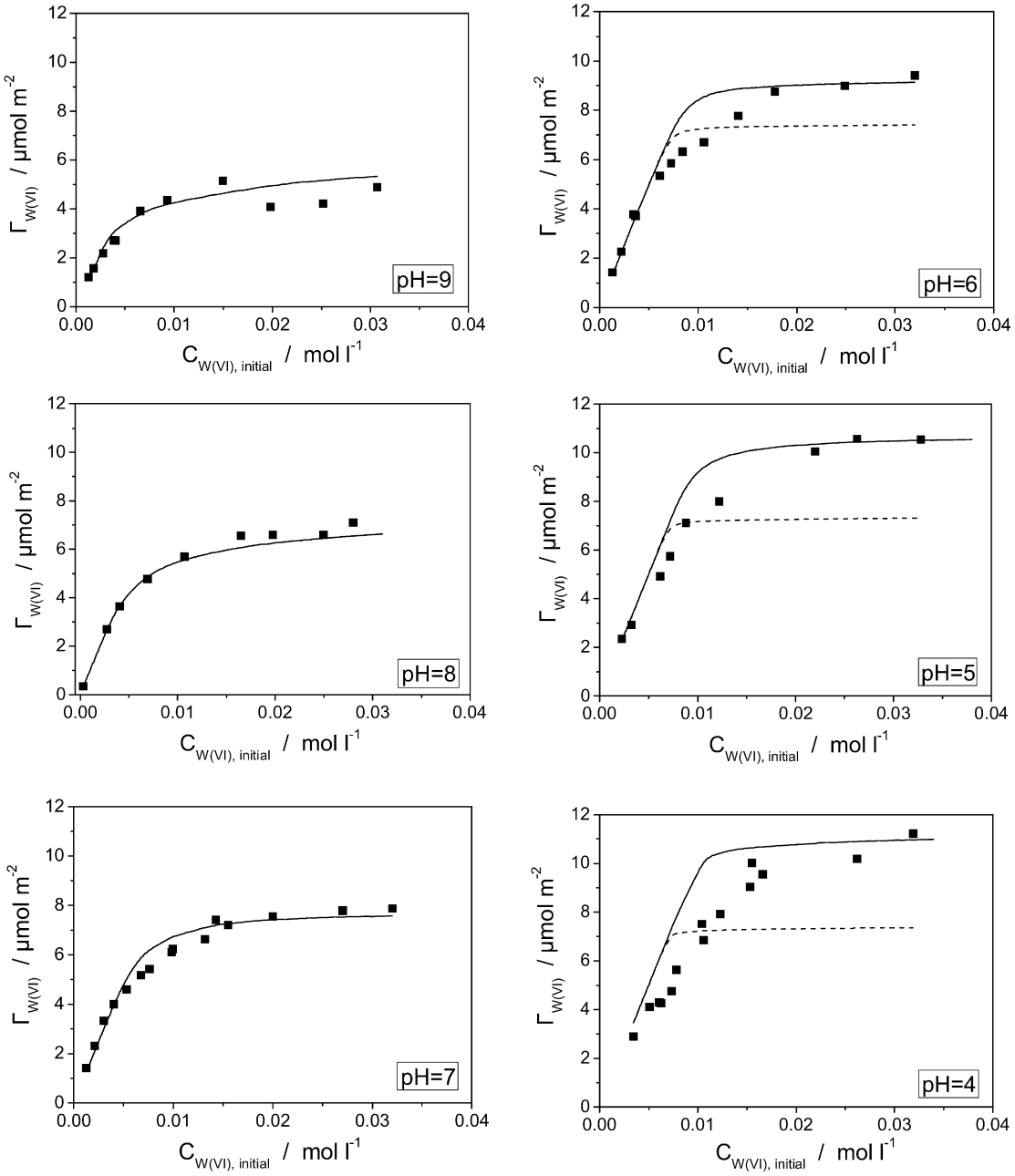

Fig. 1. Adsorption isotherms of W(VI) in the pH range 4–9. Points represent experimental data whereas solid lines correspond to calculated curves. The dashed lines were derived ignoring the deposition of tungstate polymers (see text for details).

3.4. Proton–ion titrations at constant pH

The above presented deposition methodologies are based on the examination of the deposition behavior as a function of pH, initial W(VI) concentration in the solution and proton adsorption due to this deposition. The deposition behavior and the proton adsorption may be combined quantitatively in the framework of a recently developed methodology which is based on the so-called "proton–ion titration" curves, namely linear plots of the "amount of H^+ ions adsorbed versus the amount of W(VI) deposited" [42,47]. Each of these plots is determined at a fixed pH and under conditions favoring complete deposition of the W(VI) oxo-species. The slope of each curve is equal to the ratio of the "*amount of H^+ ions adsorbed versus the amount of W(VI) deposited*."

Before presenting the aforementioned plots it is necessary to outline a correction which was performed on the experimentally determined values for the amount of the adsorbed protons. It was imposed by our W(VI) speciation in solution. Upon addition of a small volume (0.0008 dm^3) of the W(VI) solution of 0.01 M into a suspension of volume 0.1 dm^3 (see experimental part of Ref. [42]), the concentration of the W(VI) solution becomes too low (<0.0001 M). This dilution causes a transformation of the polymer into monomer W(VI) oxo-species for pHs $\leqslant$ 6 (see also Figs. A1-1–A1-4 of Appendix A1 in Supplementary material). During this transformation H^+ ions are released to the solution according to the equilibria:

$$x\mathrm{WO}_4^{2-} + n\mathrm{H}^+ \longleftrightarrow \mathrm{H}_p\mathrm{W}_x\mathrm{O}_{4x-\left(\frac{n-p}{2}\right)}^{-2x+n} + \frac{(n-p)}{2}\mathrm{H}_2\mathrm{O}. \quad (1)$$

The above lead to an under-estimation of the H^+ ions actually adsorbed on the interface upon the deposition of the W(VI) oxo-species. Taking into account the above, the determined amount

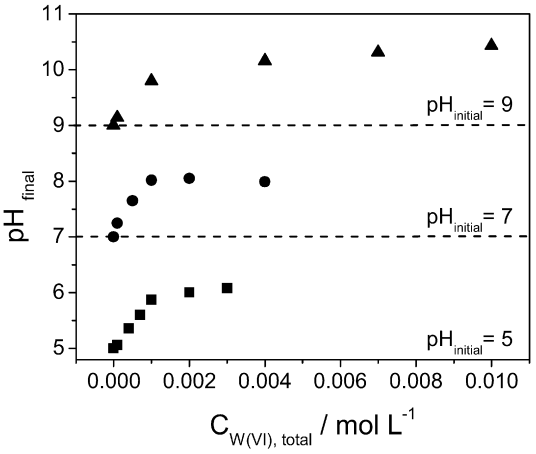

Fig. 2. Increase of pH upon the deposition of the W(VI) oxo-species at the "titania/impregnation solution" interface, for various initial W(VI) concentrations and three values of initial pH (5.0, 7.0 and 9.0).

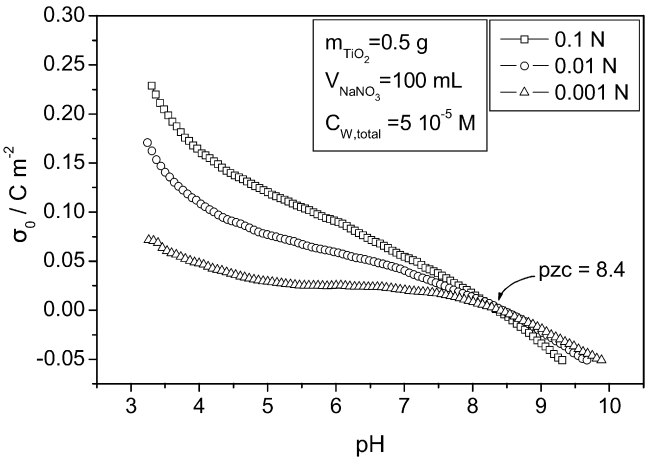

Fig. 3. "Surface charge density vs pH" curves in the presence of the W(VI) oxo-species in the impregnation solution at three different values of ionic strength.

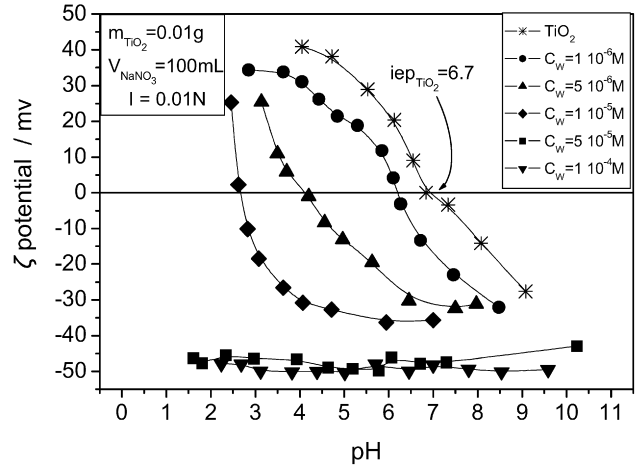

Fig. 4. "ζ potential vs pH curves" obtained both in the absence and presence of the W(VI) oxo-species in the impregnating suspension, for various initial W(VI) concentrations.

of the H^+ ions adsorbed was corrected by adding the amount of the H^+ ions released upon depolymerization. The latter was determined by performing the dilution experiments in the absence of titania and measuring the change of pH or by applying the Visual MINTEQ program (see Section 2) which solves the equilibria (1). Both approaches provided the same results. The linear plots "*amount of the H^+ ions adsorbed versus the amount of the W(VI) deposited*" obtained after the aforementioned correction are illustrated in Fig. 5.

The values obtained for the ratio $r = \Gamma_{H^+}/\Gamma_W$ at pHs 9, 8, 7, 6, 5 and 4, are respectively equal to 1.1, 1.4, 1.7, 1.8, 0.36 (1.7), and 0.11 (1.5) (Values in parentheses are corrected ones. See "Section" for details).

3.5. Laser-Raman spectroscopy

According to the literature [7,48] five peaks appear in the range 0–700 cm^{-1} for titania, four peaks due to anatase (142, 398, 517, 639 cm^{-1}) and one peak (475 cm^{-1}) due to rutile. Moreover, a very small peak (due to anatase) appears at 790 cm^{-1}. In view of the above it is clear that the range 0–700 cm^{-1} cannot be safely used for detecting the deposited W(VI) oxo-species. This is the reason for which the LR-spectra of the various $H_KW_XO_Y^{Z-}/TiO_2$ wet solid samples were recorded in the range 700–1400 cm^{-1}.

Fig. 6 shows the LR-spectra of several model compounds. In the spectrum of the solid Na_2WO_4 (Fig. 6(a)) four bands appear at 928, 835 (due to symmetric and asymmetric stretching vibrations of the W=O bond, respectively), 370 and 330 cm^{-1} (due to the bending vibrations of the W–O bond). Moreover, two bands appear around 100 cm^{-1} (due to vibrations of the solid lattice) [49,50].

It may be seen that the LR-band at 928 cm^{-1} is the most intense and thus it characterizes the WO_4^{2-} ions in the solid. This band appears (at 930 cm^{-1}) also in the LR-spectrum of the $NaNO_3$ aqueous solution containing the monomer WO_4^{2-} ions (Fig. 6(b)). The band at 1050 cm^{-1} is due to the nitrate ions. In the LR-spectrum of the solid $(NH_4)_{10}W_{12}O_{41}$ several bands appear (Fig. 6(c)). The most intense band appears at 952 cm^{-1}. This is due to symmetric stretching vibrations of the W=O bond [51,52]. This band appears at 960 cm^{-1} in the LR-spectrum of the $NaNO_3$ aqueous solution containing the polymeric $W_{12}O_{41}^{10-}$ ions (Fig. 6(d)). As already mentioned the band at 1050 cm^{-1} is due to the nitrate ions.

Fig. 7 shows the LR-spectra recorded for the various $H_KW_XO_Y^{Z-}/TiO_2$ wet solid samples. The wet solid samples were selected in the frame of the adsorption edge experiments, corresponding to an initial W(VI) concentration equal to 2.8×10^{-2} M. This corresponds to the plateau of the adsorption isotherms (Fig. 1). *It is important to note that the LR-spectra concern the W(VI) oxo-species deposited at the interface*. This is because the amount of the W(VI) oxo-species remained after filtration in the liquid inside the pores is negligible compared to that deposited at the interface. Inspection of Fig. 7 clearly shows that in the pH range 9–7 a band at ~935 cm^{-1} is detected, which indicates exclusive deposition of the WO_4^{2-} ions. It may be, moreover, observed that the decrease of pH in the range 6–4 brings about a broadening and a shift of the band to higher wavenumbers. Thus, this band is centered at about 952 cm^{-1} for the sample where the W(VI) deposition took place at pH 4 indicating deposition of polymer species. In order to further investigate the contribution of the W(VI) polymer species to the whole deposition as pH decreases, we have deconvoluted this band. The results of this deconvolution are illustrated in Fig. 8.

Inspection of this figure clearly shows that in the pH range 9–7 the only W(VI) oxo-species actually deposited are the monomer WO_4^{2-} ions, whereas in the pH range 6–4 there is an increasing contribution of the polymer species to the whole deposition as pH decreases. The above results are in general agreement with the aforementioned solution speciation of the W(VI) and show that the solution speciation determines to a large extent the interfacial speciation.

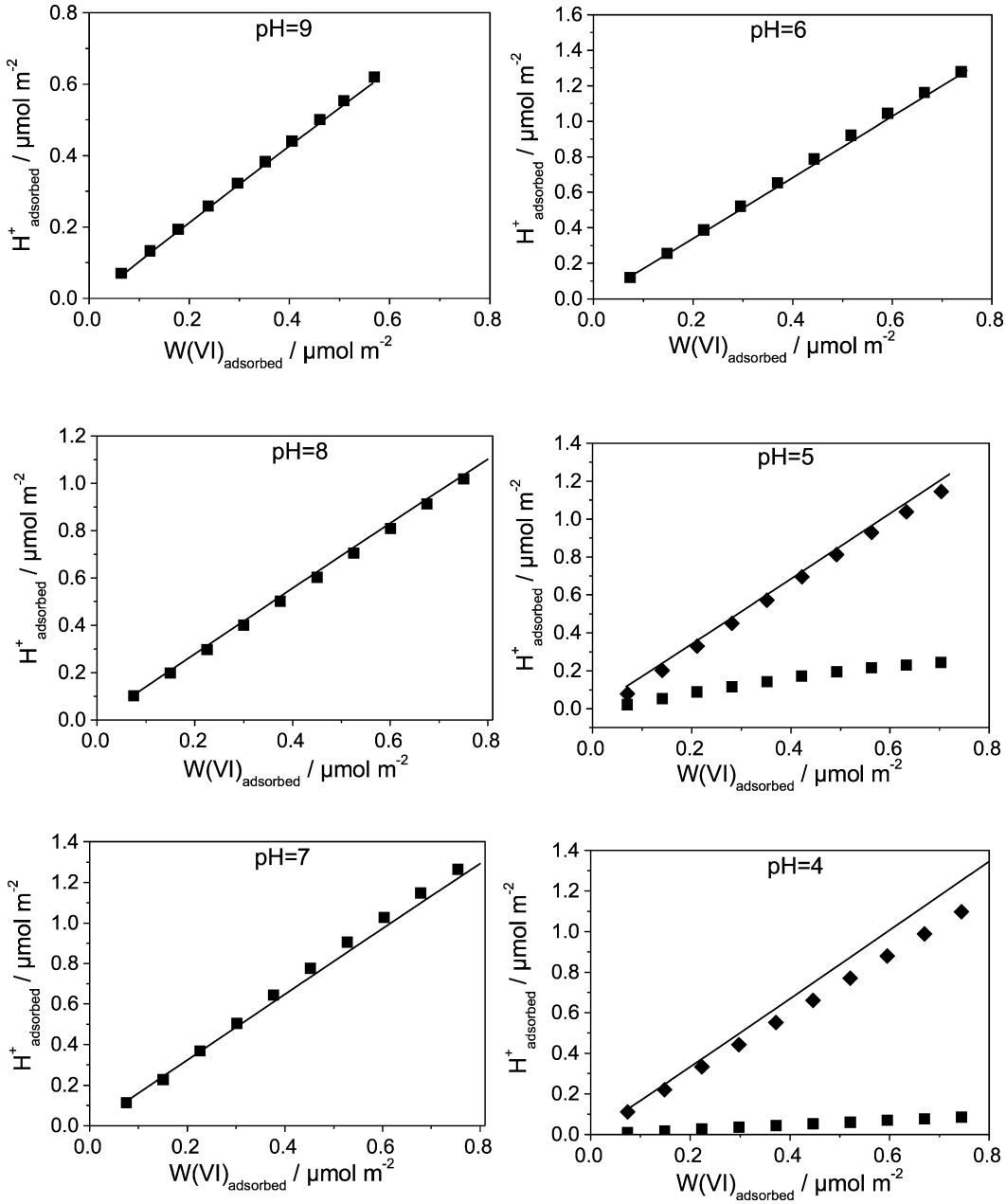

Fig. 5. Amount of the H^+ ions adsorbed vs the amount of the deposited W(VI), for various pH values. Points represent experimental data whereas solid lines correspond to calculated curves on the basis of the model established for the deposition of the W(VI) oxo-species (see below in the text). Symbol ◆ at pHs 4 and 5 represents "corrected" experimental data assuming exclusive deposition of the tungstate monomers (see "Section 4" for details).

As already mentioned the above results concern an initial W(VI) concentration equal to 2.8×10^{-2} M, corresponding to the plateau of the adsorption isotherms (Fig. 1) namely at relatively high W(VI) surface concentration (5–11 μmol m^{-2}). It is interesting to re-investigate the interfacial W(VI) speciation at low pHs and too low W(VI) surface concentrations (<1 μmol m^{-2}), corresponding to the proton–ion curves. Specifically, we investigated this speciation at pH 4 and 5 for a W(VI) surface concentration equal to 0.8 μmol m^{-2}, corresponding to an initial W(VI) concentration in the solution equal to 8×10^{-4} M. The LR results are presented in Fig. 9.

A band at 932 cm^{-1} is detected indicating the deposition of the WO_4^{2-} monomer species. On the contrary, the band at 950–960 cm^{-1} (indicative of the deposition of polymer species) is not detected. This is rather unexpected if we take into account that the aforementioned W(VI) speciation in the solution at low pHs and similar W(VI) concentration showed the presence of both monomer and polymer species. Similar results were obtained for relatively higher W(VI) surface concentrations (1.3 and 1.6 μmol m^{-2}).

3.6. Modeling the deposition process at low W(VI) surface concentrations

As already mentioned, the modeling of the deposition process attempted in the present work is based on the recently reported [38] picture for the "titania/electrolyte solution" interface in absence of the W(VI) oxo-species in the solution. This picture was briefly presented in the Introduction. Moreover, the modeling uses the values of the surface ionization and interfacial parameters obtained in the absence of the W(VI) oxo-species. These are compiled in Tables 3 (model A) and 4 of Ref. [38]. The adjustable

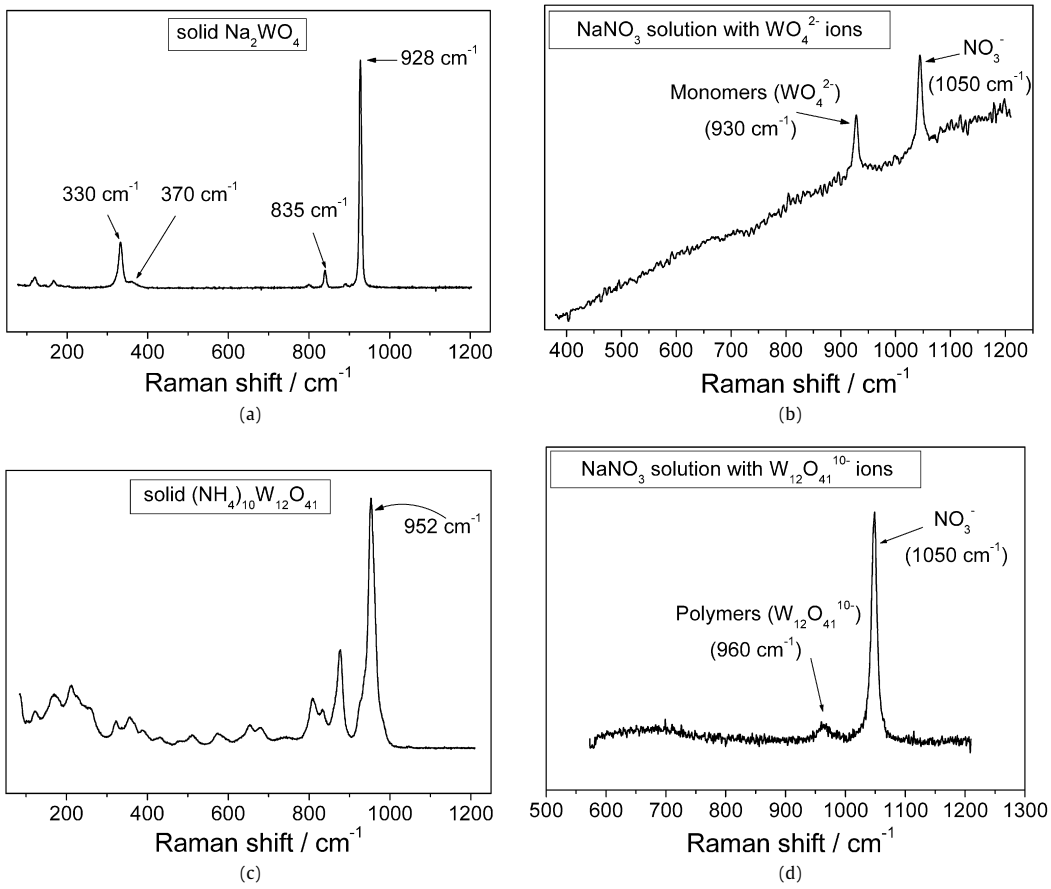

Fig. 6. LR-spectra of several model compounds: (a) solid Na_2WO_4, (b) monomer WO_4^{2-} ions in an $NaNO_3$ aqueous solution, (c) solid $(NH_4)_{10}W_{12}O_{41}$, (d) $W_{12}O_{41}^{10-}$ ions in an $NaNO_3$ aqueous solution.

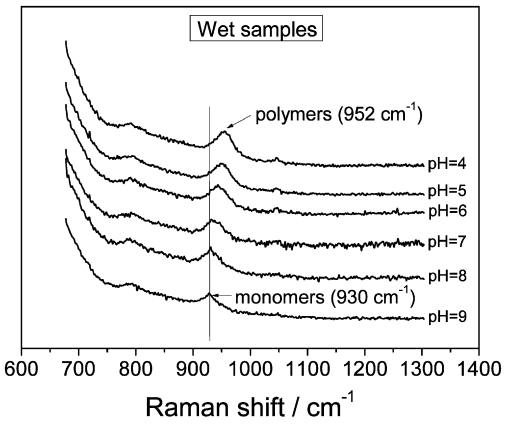

Fig. 7. LR-spectra recorded for various $H_KW_XO_Y^{Z-}/TiO_2$ wet solid samples (for details see text).

parameters in the modeling process are the following: (i) the type of the adsorption or reaction assumed between titania surface and W(VI) oxo-species (electrostatic adsorption, inner sphere formation etc.), (ii) the equilibrium constant of each adsorption/reaction and (iii) the charge distribution between the planes 0, 1 and 2 (see Section 1) for each of the deposited W(VI) oxo-species. The modeling involved an exhaustive simulation work over a large number of alternative deposition mechanisms. Details concerning the modeling process are presented in Appendix A2 of Supplementary material.

The deposition model which provided the best fitting concerning the proton–ion curves (Fig. 5) involves the following equilibria:

$$Ti_2O^{0.57-} + H^+ + WO_4^{2-} \overset{\log K_{T1}=16}{\longleftrightarrow} [Ti_2OH\cdots O\text{–}WO_3]^{1.57-}, \quad (2)$$

$$TiO^{0.35-} + 2H^+ + WO_4^{2-} \overset{\log K_{T2}=21.7}{\longleftrightarrow} TiOWO_3^{0.35-} + H_2O, \quad (3)$$

$$2TiO^{0.35-} + 4H^+ + WO_4^{2-} \overset{\log K_{T3}=31.6}{\longleftrightarrow} Ti_2O_2WO_2^{1.3+} + 2H_2O. \quad (4)$$

According to these equilibria, the monomer WO_4^{2-} ions are deposited on both the terminal and bridging surface oxygen atoms. In the first case, mono-substituted and di-substituted mononuclear inner sphere complexes are formed whereas in the second case the deposition takes place exclusively through formation of a hydrogen bond. It should be stressed that the model curves failed to fit the experimental proton–ion titrations data when it was considered formation of inner sphere complexes on the bridging oxygen atoms. This is presumably due to the fact that the surface oxygens of this kind are already doubly coordinated by two Ti atoms.

3.7. Modeling the deposition process in the whole range of W(VI) surface concentrations

Using the aforementioned constants, illustrated in the equilibria (2)–(4), we derived the adsorption isotherms achieved in the whole pH range studied (Fig. 1). Inspection of Fig. 1 shows a very good fitting in the pH range 9–7. In contrast, the model curves (dashed lines) failed to describe the deposition data in the

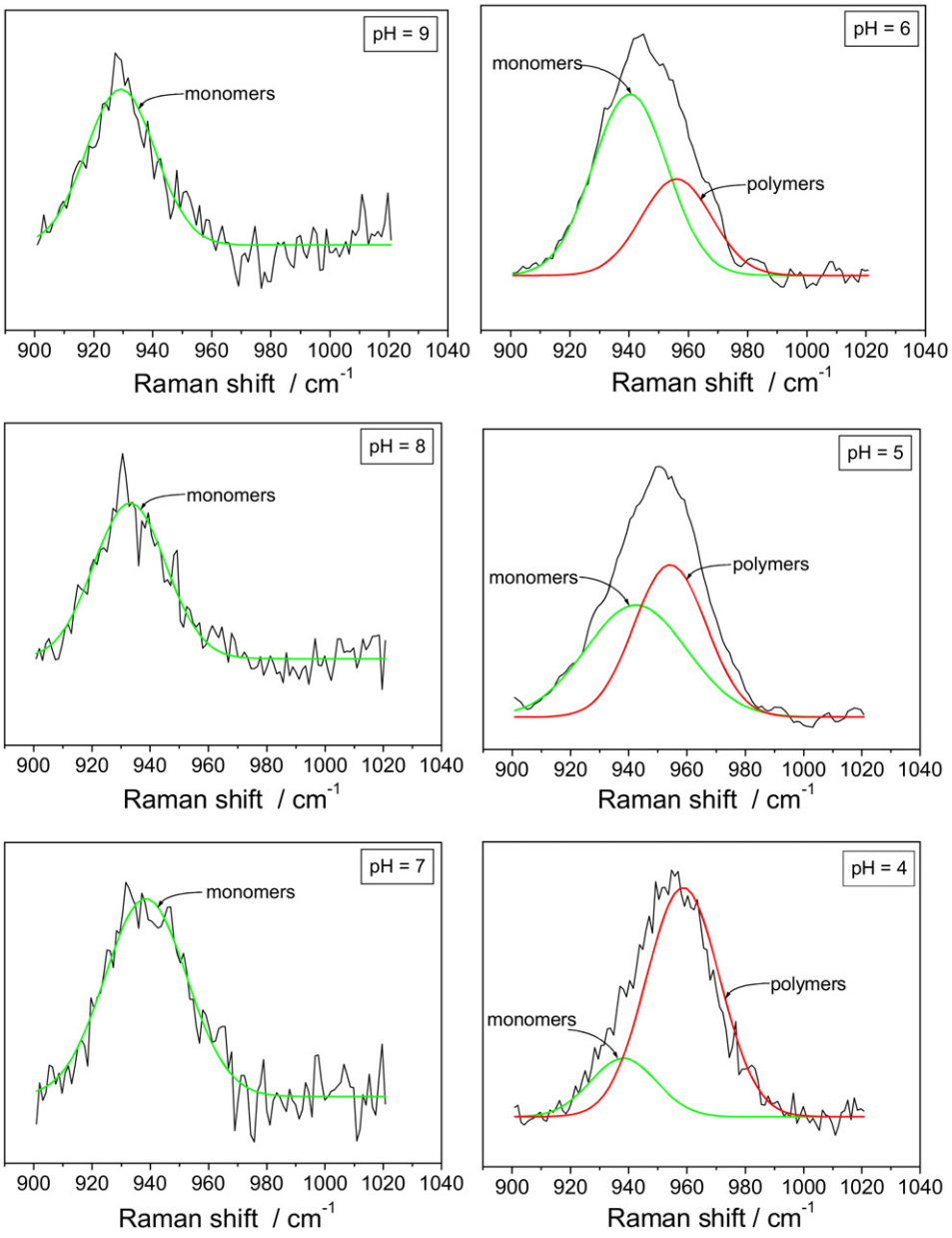

Fig. 8. Deconvolution of the broad band appeared in the range 930–952 cm^{-1} of the LR-spectra recorded for the various $H_K W_X O_Y^{Z-}/TiO_2$ wet solid samples.

pH range 6–4 and above a critical W(VI) concentration. In these cases the experimental points are located above the plateau of the model curves suggesting deposition, in addition, of the polymer species.

In view of the above we modeled the deposition process in the whole range of the pH and W(VI) concentrations adopting the formation constants for the deposited monomer species determined previously and considering the deposition, in addition, of polymer species in the pH range 6–4. As already found the main polymer species present in solution under these conditions are the $W_7O_{24}^{6-}$, $HW_7O_{24}^{5-}$ and $H_2W_{12}O_{42}^{10-}$ ions. In this step of modeling the additional adjustable parameters are the mode of interfacial deposition, the structure of the deposited polymer species and the corresponding formation constants. The best description of the experimental data (solid lines in Fig. 1) were obtained adopting the following deposition equilibria for the polymer species, in addition to those which have been adopted previously for the deposition of the monomer ones.

$$5TiO^{0.35-} + 5Ti_2O^{0.57-} + 18H^+ + 7WO_4^{2-} \overset{\log K_{T4}=164.7}{\longleftrightarrow} \left[5(TiOH)5(Ti_2OH)\ldots W_7O_{24}\right]^{0.6-} + 4H_2O, \quad (5)$$

$$5TiO^{0.35-} + 5Ti_2O^{0.57-} + 19H^+ + 7WO_4^{2-} \overset{\log K_{T5}=167.7}{\longleftrightarrow} \left[5(TiOH)5(Ti_2OH)\ldots HW_7O_{24}\right]^{0.4+} + 4H_2O, \quad (6)$$

$$7TiO^{0.35-} + 7Ti_2O^{0.57-} + 28H^+ + 12WO_4^{2-} \overset{\log K_{T6}=259.4}{\longleftrightarrow} \left[7(TiOH)7(Ti_2OH)\ldots H_2W_{12}O_{42}\right]^{2.44-} + 6H_2O. \quad (7)$$

The above equilibria indicate that the polymeric $W_7O_{24}^{6-}$, $HW_7O_{24}^{5-}$ and $H_2W_{12}O_{42}^{10-}$ species are adsorbed through electrostatic forces. The very good fitting of the experimental data (solid lines in Fig. 1) provided the values for the formation constants of the deposited polymer species (they were adjustable parameters in the modeling). These are illustrated in the equilibria (5)–(7).

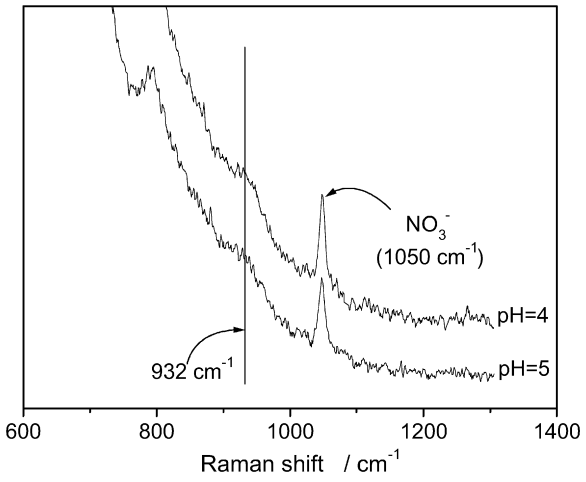

Fig. 9. LR-spectra recorded for two $H_KW_XO_Y^{Z-}/TiO_2$ wet solid samples, prepared at different pH values, at the end of the proton–ion experiments, using an initial W(VI) concentration equal to 8×10^{-4} M.

4. Discussion

4.1. The mode of interfacial deposition

The mode of interfacial deposition may be first investigated by inspecting the adsorption isotherms (Fig. 1). The fact that the surface W(VI) concentration, Γ_W, increases with the initial W(VI) concentration in the solution is easily understandable. Moreover, Γ_W increases as pH decreases. Taking into account the negative charge of the deposited W(VI) oxo-species and the fact that the surface charge of the support becomes positive below pzc (6.5), one could be inclined to believe that the deposition takes place through simple electrostatic accumulation of the W(VI) oxo-species in the diffuse part of the interface. However, this view cannot explain the observation that *considerable deposition takes place even at pH ⩾ pzc of the support (6.5) where its surface was initially neutral or negatively charged*. This observation strongly suggests some kind *of specific interactions with the receptor sites* and presumably formation of inner sphere surface complexes with the surface (hydr)oxo-groups.

Adopting this deposition mechanism we may imagine that the W(VI) oxo-species are located near to the surface, namely inside the compact layer. This means that negative charge is accumulated in this region, with consequent adsorption of protons on the surface in order to compensate this negative charge. Thus, the pH of the impregnation solution is expected to increase considerably. This prediction is confirmed experimentally as it may be seen in Fig. 2. It is remarkable that the effect is pronounced even at pH 9, where the surface is negatively charged. This implies specific interactions even in this extreme case. From the above it may be concluded that the change of pH upon the deposition of the W(VI) oxo-species at the "titania/impregnating solution" interface suggests the development of specific interactions and presumably formation of inner sphere complexes, at least for some of the deposited W(VI) oxo-species. The observation that the increase of pH appears to level off for initial concentrations >0.001 M does not mean that the deposition takes place without change of pH at high concentrations. As it will be discussed below, a preferential deposition of the tungstate monomers takes place, which shifts the equilibria (1) to the left. This means that H^+ ions are released in the solution which compensates the aforementioned adsorption of protons on the surface. Therefore, macroscopic pH stability is observed, though the deposition of tungstates is followed by proton adsorption.

As already explained, protons are adsorbed onto the surface upon deposition of the W(VI) oxo-species inside the compact layer of the interface. It is obvious that this should take place at all pH values including the pH = pzc, where the surface was neutral before deposition. Therefore, in the presence of the deposited negative species, more hydroxyls in solution are required in order to deprotonate surface groups and restore a zero proton charge at the surface. Thus, an eventual shift of the pzc of titania used (6.5) to a higher value would strongly suggest the development of specific interactions and presumably formation of inner sphere complexes. The determination of a pzc = 8.4 for a titania suspension in the presence of W(VI) oxo-species (Fig. 3) shows that this is indeed the case.

The above mentioned finding concerning the development of specific interactions between the deposited W(VI) oxo-species and the titania surface is also corroborated by the microelectrophoresis results. In Fig. 4 we may observe that the presence of the W(VI) oxo-species in the suspension decreases the ζ potential and shifts the iep to lower values This suggests accumulation of negatively charged species at the compact and/or stagnant-diffuse part of the interface through development of specific interactions and presumably formation of inner sphere complexes located inside the compact layer. In fact, when a simple electrostatic accumulation of the W(VI) oxo-species was taken place at the whole interfacial region, like that of the indifferent ions, the curves "ζ vs pH," recorded in the presence of the W(VI) oxo-species, as well as the iep value should be rather identical with those observed in the absence of these species at the same ionic strength. In contrast, when the deposition of the negative W(VI) oxo-species occurs through coordinative/hydrogen bonds which impose accumulation at the aforementioned regions of the interface, the values of the ζ potential should decrease over the whole pH range studied. On the other hand, the iep should be shifted to a lower value. This is because a surface protonation is required to restore the electrokinetic charge and thus the ζ potential, at zero value. The increase of the magnitude of these effects with the amount of the deposited W(VI) oxo-species is rather expected. Above a critical amount of the deposited W(VI) oxo-species a charge reversal is observed where ζ potential takes negative values even at pH values where the surface charge is positive. The high intensity of the effect indicates that at least some of the W(VI) oxo-species are located at the compact rather than at the stagnant-diffuse layer.

Finally, the values obtained from the proton–ion curves (Fig. 5) for the ratio $r = \Gamma_{H^+}/\Gamma_W$ are relatively large, indicating formation of mono-substituted and/or di-substituted inner sphere complexes of the deposited WO_4^{2-} ions with the surface (hydr)oxo groups [15]. The slight increase of this ratio presumably indicates increasing contribution of the di-substituted as pH decreases.

In view of the above it seems that the results coming from the deposition experiments, electrochemical techniques and proton–ion curves strongly suggest specific interactions of the W(VI) species and presumably formation of inner sphere complexes.

4.2. A qualitative analysis of the interfacial speciation of the W(VI)-oxo species by the application of laser-Raman spectroscopy

The LR investigation showed that the interfacial W(VI) speciation depends on both the W(VI) surface concentration and the solution pH. At relatively high W(VI) surface concentrations (5–11 μmol m^{-2}), corresponding to the plateau of the isotherms, and pH range 9–7 the monomer WO_4^{2-} ions are deposited (detection of one band at ~935 cm^{-1} indicative of the deposition of monomer species; see Fig. 8). In the pH range 6–4 polymer species are deposited in addition. The relative concentration of the latter increases as pH decreases (detection of an additional band at ~955 cm^{-1} indicative of the deposition of polymer

species; see Fig. 8). At relatively low W(VI) surface concentrations (<2 μmol m^{-2}) corresponding to the proton–ion curves, WO_4^{2-} monomer species are deposited exclusively even at too low pH values, where polymers are also present in the solution. This was inferred by the absence of the characteristic band of the polymer species (~955 cm^{-1}) in the LR spectra of the corresponding samples (see Fig. 9). The selectivity of the surface for the monomer species, being in full agreement with the established deposition model, may be attributed to the following three reasons: (i) The accumulation of negative charge near the surface develops negative potential, which in turn inhibits the deposition of the highly negative polymer species. (ii) Inhibition of the deposition of the polymer species due to stereochemical hindrance. (iii) Enhancement of the deposition of the monomer species due to the formation of surface coordinative bonds with respect to the electrostatic retention of the polymer species.

4.3. The local structure of the deposited W(VI) oxo-species on titania surface

The joint use of the deposition, electrochemical methodologies and proton–ion titrations suggested location of the of W(VI) oxo-species at the compact/diffuse-stagnant part of the "titania/impregnation solution" interface and presumably formation of inner sphere complexes. On the other hand, the application of laser-Raman spectroscopy allowed an approximate interfacial speciation. The exact local structure at low W(VI) surface concentrations of the deposited W(VI) monomer species was fully elucidated by simulating the proton–ion curves on the basis of a deposition model. As already mentioned in Section 3, the deposition model was obtained after exhaustive simulation of various alternatives concerning the deposition mechanism. In the simulation work we took into account the aforementioned finding concerning the interfacial location of the of W(VI) oxo-species and the nature of the surface bonds. The developed model (equilibria (2)–(4)) provided the best fitting concerning the proton–ion curves (Fig. 5).

In this point it should be mentioned that initially, we had assumed that there was no selectivity in the deposition of the W(VI) monomers at the interface. Following this assumption there was no way to fit the experimental "proton–ion" results at pHs 4 and 5, for any mode of interfacial deposition and distribution of the ions charge in the interface. In both cases the model curves predicted considerably higher $H^+_{ads}/W(VI)_{ads}$ ratio than the experimental one (compare points ■ with the model curves for pHs 4 and 5 in Fig. 5). In view of the above it was reasonable to think that the too low experimental $H^+_{ads}/W(VI)_{ads}$ ratio could be due to the selective deposition of the tungstate monomers, in the range of the W(VI) concentration in which the "proton–ion" experiments have been performed. In such a case the equilibria (1) would be shifted to the left. Therefore, the selective deposition of the WO_4^{2-} ions causes a release of the H^+ ions in the solution resulting to an *underestimation* of the H^+ ions adsorbed on the surface upon the deposition of the W(VI) oxo-species. Thus, the only way to obtain an agreement between the model predictions and the experimental results was to assume exclusive deposition of the WO_4^{2-} species and correct properly the experimental points taking into account the aforementioned equilibria.

Thus, the amount of the adsorbed protons was again calculated by taking into account the equilibria (1) and applying the Visual MINTEQ program. Moreover, this amount was determined experimentally by performing the same experiments for obtaining the proton–ion curves (described in the experimental part) but using W(VI) solutions at pH 7 which contain only monomer W(VI) species. Both approaches provided the same results. The so calculated (or determined) amount of the H^+ ions was also added to the experimentally determined amount of the H^+ ions adsorbed upon the deposition of the W(VI) oxo-species. The linear plots "*amount of the H^+ ions adsorbed versus the amount of the W(VI) deposited*" for pHs 4 and 5, resulted after the aforementioned correction, are illustrated in Fig. 5 with different symbols (◆). The very good agreement between the "corrected" experimental data and the model curves corroborated the finding of the LR spectra that exclusive deposition of the WO_4^{2-} monomeric species takes place at low W(VI) surface concentrations, corresponding to the proton–ion curves, even at too low pH values. Thus, the model of the deposition for low W(VI) concentration is in full agreement with all the experimental results.

As already mentioned this model predicted the formation of mono-substituted and di-substituted inner sphere complexes with the terminal oxygen atoms and location through hydrogen bond with the bridging surface oxygen atoms. Moreover, this model predicted that the deposited species are located inside the compact layer of the interface. Specifically, in all configurations the W atom is situated between the surface plane and plane 1, whereas the solution oriented oxygen atoms are situated at plane 1 of the compact layer. The charge of the deposited monomer species is distributed between the surface plane and plane 1. A schematic representation of the local structures of the deposited species is illustrated in Fig. 10. The anatase (1 0 0) crystal termination, one of the two major crystal faces of anatase, has been chosen to exemplify these structures. Similar pictures may be obtained by considering the other major crystal termination of the anatase (1 0 1).

As already mentioned, having successfully described the experimental "proton–ion" curves, we then attempted to model the deposition process *in the whole W(VI) surface concentration* range by describing the experimental deposition isotherms as well. The best description (see Fig. 1) was achieved by adopting the equilibria (5)–(7), in addition to the equilibria (2)–(4). A schematic representation of the local structure of the deposited $W_7O_{24}^{6-}/HW_7O_{24}^{5-}$ species is illustrated in Fig. 11 taking into account the equilibria (5) and (6) and that the model predicted adsorption sites involving five bridging and five terminal neighboring (hydr)oxo groups. The anatase (1 0 1) crystal termination, one of the two major crystal faces of anatase, has been chosen to exemplify this structure. Similar picture may be obtained by considering the other major crystal termination of the anatase (1 0 0).

The surface covered by $W_7O_{24}^{6-}/HW_7O_{24}^{5-}$ species was calculated on the basis of crystallographic data relevant to the W–O bond lengths and the geometry of these polymeric ions [53,54]. This was found to be equal to 0.7 nm^2 including 10 bridging and terminal neighboring (hydr)oxo groups. Therefore, from the stereochemical point of view, the structure illustrated in Fig. 11 is quite reasonable.

A schematic representation of the local structure of the deposited $H_2W_{12}O_{42}^{10-}$ species is illustrated in Fig. 12 taking into account the equilibria 7 and that the model predicted adsorption sites involving 7 bridging and 7 terminal neighboring (hydr)oxo groups. The anatase (1 0 1) crystal termination, one of the two major crystal faces of anatase, has been chosen to exemplify this structure. Similar picture may be obtained by considering the other major crystal termination of the anatase (1 0 0).

The structure illustrated in Fig. 12 is quite reasonable from a stereochemical point of view. This is because the surface covered by the $H_2W_{12}O_{42}^{10-}$ species, calculated on the basis of the aforementioned crystallographic data [55], was found to be 1.2 nm^2, including 14 bridging and terminal neighboring (hydr)oxo groups.

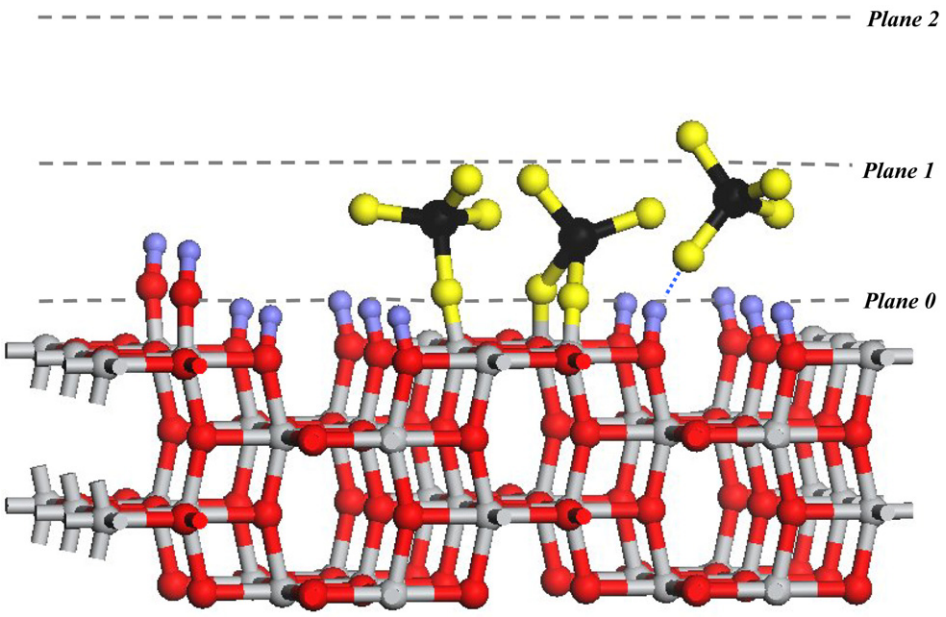

Fig. 10. Local structures of the adsorbed W(VI) monomer oxo-species on the (1 0 0) crystal termination of anatase. Ti atoms: gray balls; H atoms: blue balls; O atoms in TiO_2 cluster: red balls; O atoms in tungsten surface species: yellow balls; W atoms: black balls. The dashed line indicates H-bond. (For interpretation of the references to color in this figure legend, the reader is referred to the web version of this article.)

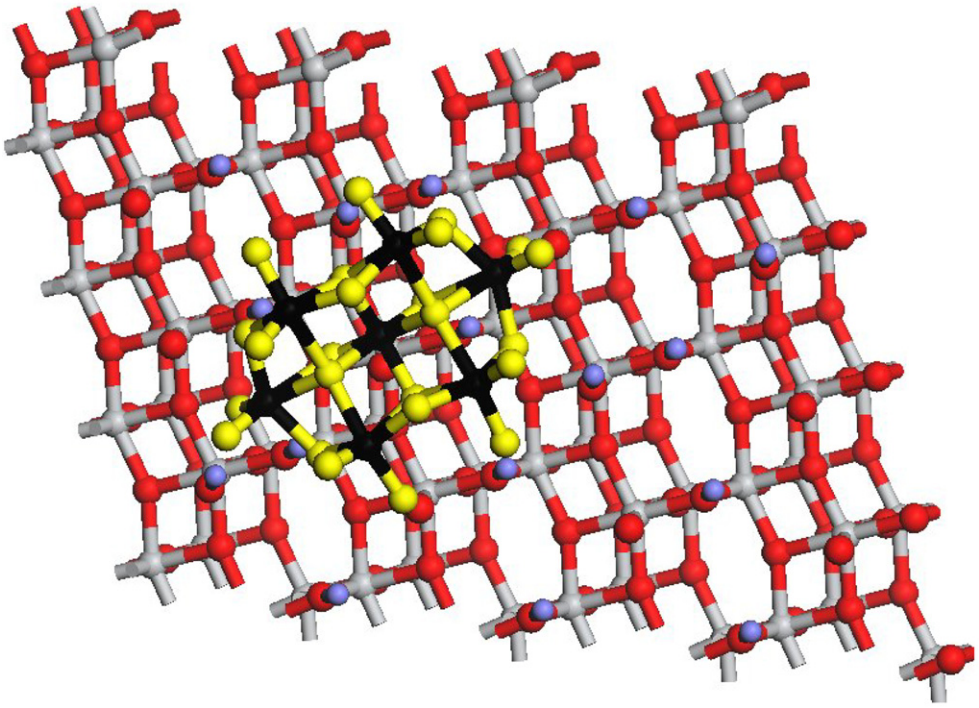

Fig. 11. Local structure of the electrostatically adsorbed $W_7O_{24}^{6-}$ species on the (1 0 1) crystal termination of anatase. For the notation see the legend of Fig. 10.

4.4. A quantitative analysis of the interfacial speciation of the W(VI)-oxo species resulted by the successful modeling of the deposition process

The determination of the values for the formation constants of the deposited monomer and polymer species allowed the calculation of the interfacial speciation for any value of the main impregnation parameters, that is for any value of pH and the W(VI) concentration in the solution (see Appendix A2 in Supplementary material). *It is understandable that it is an effective preparative tool for imposing the deposition of desired relative amounts of the W(VI) species on the titania surface and obtaining thus a severe control of the impregnation step related to the equilibrium deposition filtration technique*. In order to render this speciation more useful from the stand point of catalyst preparation, we have expressed it as the percentage of the deposited W(VI) belonging to a certain W(VI) oxo-species. In Fig. 13 it is presented, as an example, the interfacial speciation over a wide pH range and for two W(VI) initial concentrations in the impregnating solution.

Inspection of Fig. 13(a) shows that at relatively low initial W(VI) concentration ($\leqslant 10^{-3}$ M) practically all the adsorbed W(VI) is deposited as monomer WO_4^{2-} species, irrespective of the im-

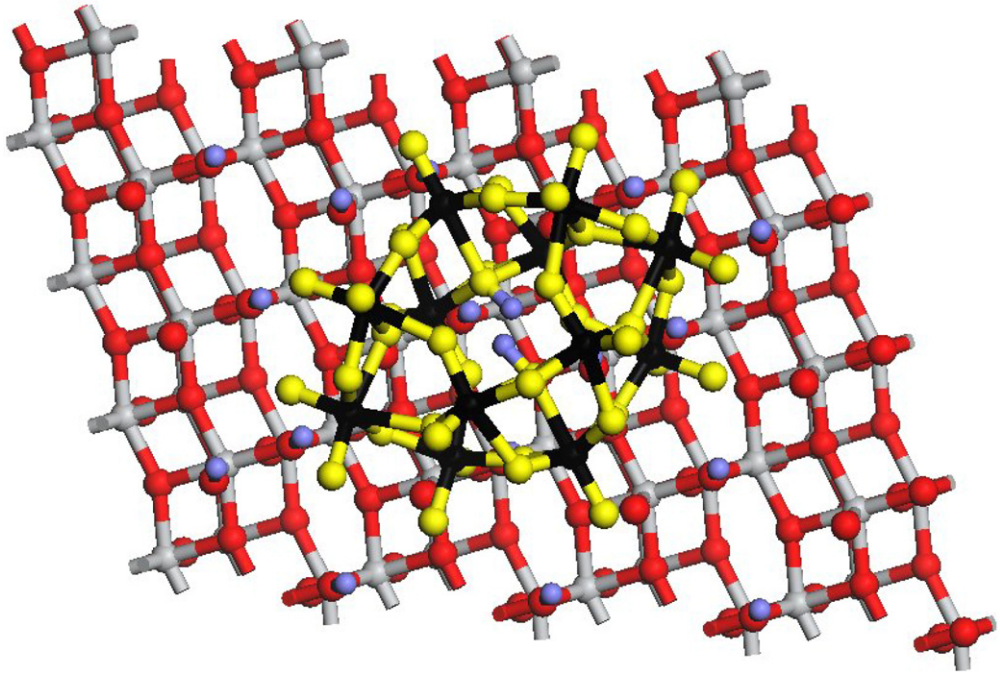

Fig. 12. Local structure of the electrostatically adsorbed $H_2W_{12}O_{42}^{10-}$ species on the (1 0 1) crystal termination of anatase. For the notation see the legend of Fig. 10.

pregnation pH. This is in line with the preferential deposition of the monomer species mentioned above. This preferential deposition becomes more pronounced if the interfacial deposition is expressed in terms of the moles of each deposited species. Concerning the speciation of the monomer species it may be observed that in the pH range 4–8 there is a preferential formation of the mono-substituted inner sphere complexes above the terminal surface oxygens, while at pHs higher than 8 the deposition through hydrogen bonds above the bridging surface oxygens becomes more important. It may be, moreover, observed that the contribution of the di-substituted inner sphere complexes above the terminal surface oxygens is very small in the whole pH range studied. Thus, our results show that one may design the preparation of the W(VI)/TiO_2 catalyst at a molecular level. For example, adopting an initial W(VI) concentration in the solution equal to 10^{-3} M and a pH equal to 4, we may deposit selectively, mono-nuclear, mono-substituted inner sphere complexes above the terminal surface oxygens.

Inspection of Fig. 13(b) shows that even at high W(VI) concentrations only the monomer species are deposited in the pH range 7–9. The contribution of the deposition of the monomer species to the whole deposition is very important even in the pH range 4–7 due to the higher deposition selectivity of these species. The interface speciation concerning these species is not very different compared to that described above for the lower W(VI) concentrations. The increase in the W(VI) concentration causes an increase of the relative amount of the deposited W(VI) through the electrostatically retained polymer species in the pH range 7–4. It may be seen that in this pH range more $W_7O_{24}^{6-}$ and $HW_7O_{24}^{5-}$ species are deposited with respect to the $H_2W_{12}O_{42}^{10-}$ species. It is evident that this trend becomes more pronounced if one expresses speciation in terms of the moles of the deposited species.

Comparison of the solution with the surface speciation of the polymer species (Fig. A1–4 in Appendix A1 of Supplementary material and Fig. 13(b)) obtained under similar conditions indicates a preferential deposition of the $W_7O_{24}^{6-}$ and $HW_7O_{24}^{5-}$ species with respect to the $H_2W_{12}O_{42}^{10-}$ species. This may be attributed to the fact that the undesired accumulation of high negative charge in the interfacial region due to the deposition of the polymer species favors the deposition of the less charged $W_7O_{24}^{6-}$ and $HW_7O_{24}^{5-}$ species with respect to the $H_2W_{12}O_{42}^{10-}$ ones. It may be, moreover, observed that the contribution of the $W_7O_{24}^{6-}$ deposition to the whole deposition is maximized at pH about 6 and then it decreases whereas the corresponding contribution of the $HW_7O_{24}^{5-}$ increases monotonically as pH decreases. This could be also partly attributed to the lower charge of the latter compared to the former.

4.5. Comparison of the main findings drawn from this study with relevant results from the literature

In the previous section we mentioned that one may take in advantage the above results in order to control the impregnation step and to some extent the whole preparation procedure. This mainly concerns the case where the EDF technique is used. Using this technique, one may control *independently* the two more important impregnation parameters: pH and solution concentration of the W(VI) oxo-species. Thus, one may impose to some extent the desirable W(VI) species deposited for obtaining a given loading of the active element. Following the more popular method of the IWI, used in the most important works concerning the W(VI) catalysts [28,29,51,56–59], the pH of the solution inside the pores of the support is largely determined by the pzc of the titania which is equal to ~6.5.

Another difference is that using EDF the deposition is practically accomplished in the equilibration step, whereas using IWI a considerable amount of the W(VI) oxo-species is deposited upon drying. Therefore, a direct comparison of our results with those obtained after IWI (before dehydration) is not so easy. The deposition model developed could be in principle extended to describe the deposition related to the IWI, though the kinetics of deposition together with the kinetics of drying should be also taken into account. This could be the subject of a future study. However, our results are in general agreement with the literature ones taken from samples prepared by IWI [51]. In both cases and for sub-monolayer surface concentrations, the deposition of

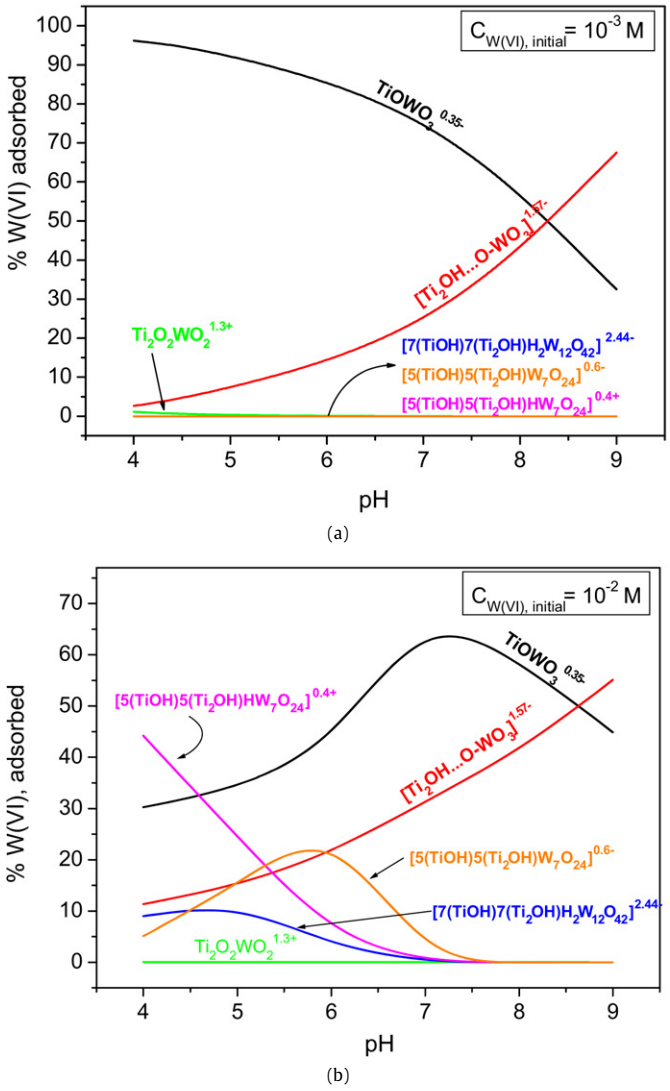

Fig. 13. Variation of the % W(VI) belonging to a given adsorbed W(VI) oxo-species with the pH of the impregnating solution at $I = 0.1$ M. (a) $C_{W(VI),initial} = 10^{-3}$ M, (b) $C_{W(VI),initial} = 10^{-2}$ M. The various adsorbed W(VI) oxo-species are indicated.

monomer/polymer species is observed with an increasing deposition of the latter as the W(VI) concentration increases. This trend is also observed for the deposition of the W(VI) oxo-species on various supports [56]. On the other, the increase of the *interfacial* concentration of the polymers with decreasing pH, resulted from the present work, is in line with the Wachs' observation that this trend is followed as the pzc of the support decreases, because as already mentioned pzc determines pH in the IWI technique [56].

There are three novel findings drawn from the present study: the exact surface structure of the deposited monomer species, the determination of the exact interfacial speciation and the selectivity of the titania surface for monomer species. The model developed cannot be applied for the description of other supported catalysts. The development of a deposition model for each supported catalyst is inevitable. In this context, we have recently accomplished our study for the Mo(VI), Cr(VI), V(VI), Co(II) and Ni(II) species supported on titania.

According to the literature the calcination of the samples prepared by IWI causes a transformation of the deposited monomer and polymer species into a highly distorted octahedral coordinated structure which possesses one short W=O bond, one long opposing W–O bond and four W–O bridging bonds [51]. This was manifested by the disappearance of the Raman peak at 935 cm^{-1} and the appearance of a sharp one at about 1010 cm^{-1} [51]. The shift of the latter peak from 1007 to 1020 cm^{-1} with the surface W(VI) concentration was attributed later to the increasing contribution of the polymer supported species [28,29]. Similar transformations of the W(VI) oxo-species due to the calcination have been reported for other supports (formation of $O_4W{=}O$, $O_2W{=}(O)_2$ monotungstes as well as polytungstates species) [28,29,56–59].

In view of the above it is clear that a direct comparison of the surface structures established in the present work with the ones formed after dehydration for the samples prepared by IWI is extremely difficult. However, the prediction of the model for the increasing interfacial concentration of the polymer W(VI) species with the W(VI) loading seems to be preserved after dehydration. On the other hand, the structures proposed in the present study for the supported monomer species could be the intermediate structures between the ions being in the solution and the final (after calcination) supported structures. In fact, it seems to us reasonable that the hydrogen bond transforms into a coordinative surface bond and an increase in the number of these bonds occurs (Fig. 10) on heating of the samples to relatively high temperatures. In any case more research is required in order to investigate the evolution of the supported species, established in the present work for samples prepared by *using equilibrium deposition filtration*, with the heating temperature.

5. Conclusions

The following conclusions may be drawn from the present work:

1. The monomer, WO_4^{2-}, ions are exclusively deposited at the "titania/electrolytic solution" interface at relatively low W(VI) concentrations of the impregnation solution ($\leqslant 10^{-3}$ M) and over the whole pH range studied (9–4).
2. Three different monomer species are formed: an inner sphere mono-substituted complex with the terminal surface oxygen atoms of titania ($TiO{-}WO_3^{0.35-}$), a surface species where the WO_4^{2-} ions are retained above a bridging surface hydroxyl through a hydrogen bond ($Ti_2OH\ldots O{-}WO_3^{1.57-}$) and an inner sphere di-substituted complex with two terminal surface oxygen atoms of titania ($Ti_2O_2WO_2^{1.3+}$).
3. In the pH range 4–8 there is a preferential formation of the mono-substituted inner sphere complexes above the terminal surface oxygens, while at pHs > 8 the deposition through hydrogen bonds above the bridging surface hydroxyls becomes more important. The interfacial concentration of the di-substituted inner sphere complexes above the terminal surface oxygens is observable only at pHs close to 4.
4. At relatively high W(VI) concentrations of the impregnation solution ($>5 \times 10^{-3}$ M) polymer W(VI) oxo-species ($W_7O_{24}^{6-}$, $HW_7O_{24}^{5-}$ and $H_2W_{12}O_{42}^{10-}$) are formed at the "titania/electrolytic solution" interface in the pH range 7–4, in addition to the aforementioned monomer W(VI) oxo-species. On the contrary, only the monomer species are formed in the pH range 9–7.
5. The polymer species are adsorbed through electrostatic forces. Concerning the deposition of the $W_7O_{24}^{6-}/HW_7O_{24}^{5-}$ species, the adsorption sites involve 5 bridging and 5 terminal neighboring (hydr)oxo groups whereas the sites relevant to the deposition of the $H_2W_{12}O_{42}^{10-}$ species involve 7 bridging and 7 terminal neighboring (hydr)oxo groups.
6. The interfacial speciation of the monomer species are similar for low and high W(VI) concentrations of the impregnation solution.

7. Concerning the interfacial speciation of the polymer species in the pH range 7–4 more $W_7O_{24}^{6-}$ and $HW_7O_{24}^{5-}$ species are deposited with respect to the $H_2W_{12}O_{42}^{10-}$ species. The contribution of the $W_7O_{24}^{6-}$ deposition to the whole deposition is maximized at pH about 6 and then it decreases whereas the corresponding contribution of the $HW_7O_{24}^{5-}$ increases monotonically as pH decreases.
8. Comparison of the solution with the interface speciation indicated a preferential deposition of the monomer WO_4^{2-} ions with respect to the polymer ones.
9. The aforementioned deposition features namely the mode of interfacial deposition, the interfacial speciation and the structure of the deposited W(VI) oxo-species may be very useful for controlling the impregnation step related to the equilibrium deposition filtration technique.

Supplementary material

The online version of this article contains additional supplementary material.

Please visit DOI: 10.1016/j.jcat.2009.01.003.

References

[1] K. Bourikas, Ch. Fountzoula, Ch. Kordulis, Appl. Catal. B 52 (2004) 145.
[2] L. Lietti, J. Svachula, P. Forzatti, G. Busca, G. Ramis, P. Bregan, Catal. Today 17 (1993) 131.
[3] M. Kobayashi, K. Miyoshi, Appl. Catal. B 72 (2007) 253.
[4] F. Bertinchamps, A. Attianese, M.M. Mestdagh, E.M. Gaigneaux, Catal. Today 112 (2006) 165.
[5] Z. Ma, W. Hua, Y. Tang, Z. Gao, Chem. Lett. 11 (1999) 1215.
[6] F. Witzel, G. Pajonk, S. Fischer, PCT Int. Appl. (2000) 17.
[7] J. Ramirez, G. Macias, L. Cedeno, A. Gutierrez-Alejandre, R. Cuevas, P. Castillo, Catal. Today 98 (2004) 19.
[8] X. Chen, S. Li, Y. Wang, Fenzi Cuihua 14 (2000) 245.
[9] C. Martin, G. Solana, V. Rives, G. Marci, L. Palmisano, A. Sclafani, Catal. Lett. 49 (1997) 235.
[10] Y. Cheng, Y. Zhang, Y. Tang, Cuihua Xuebao 22 (2001) 203.
[11] Y.R. Do, W. Lee, K. Dwight, A. Wold, J. Solid State Chem. 108 (1994) 198.
[12] J.R. Sohn, H.S. Cho, H.W. Kim, J. Ind. Eng. Chem. 5 (1999) 1.
[13] W. Grunert, R. Feldhaus, K. Anders, E.S. Shpiro, K.M. Minachev, J. Catal. 120 (1989) 444.
[14] T. Yamaguchi, Y. Tanaka, K. Tanabe, J. Catal. 65 (1980) 442.
[15] K. Bourikas, Ch. Kordulis, A. Lycourghiotis, Catal. Rev. 48 (2006) 363.
[16] T. Ataloglou, J. Vakros, K. Bourikas, Ch. Fountzoula, Ch. Kordulis, A. Lycourghiotis, Appl. Catal. B 57 (2005) 299.
[17] K. Bourikas, J. Vakros, Ch. Fountzoula, Ch. Kordulis, A. Lycourghiotis, Catal. Today 128 (2007) 138.
[18] L. Jiao, Y. Zha, X. Hao, J.R. Regalbuto, Stud. Surf. Sci. Catal. 162 (2006) 211.
[19] J.T. Miller, M. Schreier, A.J. Kropf, J.R. Regalbuto, J. Catal. 225 (2004) 203.
[20] L. D'Souza, L. Jiao, J.R. Regalbuto, J.T. Miller, A.J. Kropf, J. Catal. 248 (2007) 165.
[21] J.A. Bergwerff, M. Jansen, B.G. Leliveld, T. Visser, K.P. de Jong, B.M. Weckhuysen, J. Catal. 243 (2006) 292.
[22] L.G.A. Van de Water, G.L. Bezemer, J.A. Bergwerff, M. Versluijs-Helder, B.M. Weckhuysen, K.P. de Jong, J. Catal. 242 (2006) 287.
[23] F. Dumond, E. Marceau, M. Che, J. Phys. Chem. C 111 (2007) 4780.
[24] Ke-Q. Sun, E. Marceau, M. Che, Phys. Chem. Chem. Phys. 8 (2006) 1731.
[25] M.L. Toebes, M.K. van der Lee, L.M. Tang, M.H. Huis in't Veld, J.H. Bitter, A.J. van Dillen, K.P. de Jong, J. Phys. Chem. B 108 (2004) 11611.
[26] G.L. Bezemer, P.B. Radstake, V. Koot, A.J. van Dillen, J.W. Geus, K.P. de Jong, J. Catal. 237 (2006) 291.
[27] G. Ramis, G. Busca, C. Cristiani, L. Lietti, P. Forzatti, F. Bregani, Langmuir 8 (1992) 1744.
[28] I.E. Wachs, T. Kim, E.I. Ross, Catal. Today 116 (2006) 162.
[29] T. Kim, A. Burrows, C.J. Kiely, I.E. Wachs, J. Catal. 246 (2007) 370.
[30] T. Onfroy, G. Clet, S.B. Bukallah, T. Visser, M. Houalla, Appl. Catal. A 298 (2006) 80.
[31] A. Gutierrez-Alejandre, J. Ramirez, G. Busca, Catal. Lett. 56 (1998) 29.
[32] L. Karakonstantis, Ch. Kordulis, A. Lycourghiotis, Langmuir 8 (1992) 1318.
[33] L. Karakonstantis, K. Bourikas, A. Lycourghiotis, J. Catal. 162 (1996) 295.
[34] N. Spanos, J. Phys. Chem. 103 (1999) 1890.
[35] K. Bourikas, H. Matralis, Ch. Kordulis, A. Lycourghiotis, J. Phys. Chem. 100 (1996) 11711.
[36] N. Spanos, J. Catal. 183 (1999) 400.
[37] X. Carrier, J.-B. d'Espinose de la Caillerie, J.-F. Lambert, M. Che, J. Am. Chem. Soc. 121 (1999) 3377.
[38] G.D. Panagiotou, Th. Petsi, K. Bourikas, Ch.S. Garoufalis, A. Tsevis, N. Spanos, Ch. Kordulis, A. Lycourghiotis, Adv. Colloid Interface Sci. 142 (2008) 20.
[39] X. Carrier, E. Marceau, M. Che, Pure Appl. Chem. 78 (2006) 1039.
[40] N. Spanos, I. Georgiadou, A. Lycourghiotis, J. Colloid Interface Sci. 172 (1995) 374.
[41] C. Contescu, V.T. Popa, J.A. Schwarz, J. Colloid Interface Sci. 180 (1996) 149.
[42] K. Bourikas, T. Hiemstra, W.H. Van Riemsdijk, J. Phys. Chem. B 105 (2001) 2393.
[43] Z. Marczenko, Spectrophotometric Determination of Elements, Wiley, New York, 1970, p. 569. C.G. Ransay, Translation Ed.
[44] K. Bourikas, J. Vakros, Ch. Kordulis, A. Lycourghiotis, J. Phys. Chem. B 107 (2003) 9441.
[45] K. Bourikas, Ch. Kordulis, A. Lycourghiotis, Environ. Sci. Technol. 39 (2005) 4100.
[46] J.P. Gustafsson, Visual MINTEQ ver. 2.40, Department of Land and Water Resources Engineering, Royal Institute of Technology, Stockholm, 2005.
[47] R.P.J.J. Rietra, T. Hiemstra, W.H. Van Riemsdijk, Geochim. Cosmochim. Acta 63 (1999) 3009.
[48] A. Scholz, B. Schnyder, A. Wokaun, J. Mol. Catal. A Chem. 138 (1999) 249.
[49] S.S. Chan, I.E. Wachs, L.L. Murrell, C.N. Dispenziere Jr., J. Catal. 92 (1985) 1.
[50] J.A. Horsley, I.E. Wachs, J.M. Brown, G.H. Via, F.D. Hardcastle, J. Phys. Chem. 91 (1987) 4014.
[51] M.A. Vurman, I.E. Wachs, A.M. Hirt, J. Phys. Chem. 95 (1991) 9928.
[52] J. Aveston, Inorg. Chem. 3 (1964) 981.
[53] K. Pavani, A. Ramanan, Eur. J. Inorg. Chem. (2005) 3080.
[54] P. Roman, J.M. Gutierrez-Zorrilla, M. Martinez-Ripoll, S. Garcia-Blanco, Transition Met. Chem. 11 (1986) 143.
[55] J.J. Crywagen, I.F.J. Van der Merwe, L.R. Nassimbeni, M.L. Niven, E.A. Symonds, J. Chem. Crystallogr. 16 (1986) 525.
[56] E.I. Ross-Medgaarden, I.E. Wachs, J. Phys. Chem. C 111 (2007) 15089.
[57] B.M. Weckhuysen, J.-M. Jehng, I.E. Wachs, J. Phys. Chem. B 104 (2000) 7382.
[58] M.M. Ostromecki, L.J. Burcham, I.E. Wachs, J. Mol. Catal. A Chem. 132 (1998) 59.
[59] D.S. Kim, M. Ostromecki, I.E. Wachs, J. Mol. Catal. A Chem. 106 (1996) 93.